Comparative structural study of the disordered MCd_6 quasicrystal approximants

Cesar Pay Gómez* and Sven Lidin
Inorganic Chemistry, Arrhenius Laboratory, Stockholm University, S-106 91 Stockholm, Sweden
(Received 19 February 2003; published 17 July 2003)

Several of the MCd_6 approximants (M=Pr, Nd, Sm, Eu, Gd, Dy, Yb, Y, and Ca) to the $MCd_{5.7}$ quasicrystals (M=Yb and Ca) have been synthesized and their structures have been refined from single-crystal x-ray-diffraction data; the different types of disorder of the central Cd_4 tetrahedra located in the dodecahedral cavities of these closely related compounds have been examined and mutually compared. A model that describes this disorder and can be applied to all the examined MCd_6 phases has been elaborated. The refinements made on these phases differ from what is found in previous reports.

DOI: 10.1103/PhysRevB.68.024203 PACS number(s): 61.66.Dk, 61.44.Br, 61.10.Nz

I. INTRODUCTION

Bruzzone *et al.* and Wang did most of the early work on the cubic MCd_6 and structurally related hexagonal $RE_{13}(Cd/Zn)_{58}$ (RE=rare earth) phases in the 1970s,[1,2] more than fifteen years before the concept of quasicrystallinity was known.[3] The phases were mainly characterized by powder methods and often no refinements were made. A closer examination of the early literature reveals many ambiguities in the structural descriptions of these related compounds; different types of structures have in several cases been used to describe the same compound. The prototype structure assigned to the MCd_6 phases are YCd_6, $YbCd_6$, and Ru_3Be_{17}.[4–6] The skeletal networks of these three types of structures are identical; the difference between them lies solely in their description of the species residing inside the central dodecahedral cavity that is found in all the MCd_6 phases. In the case of Ru_3Be_{17} the cavity is reported to be empty, while in the other prototype structures it contains a Cd_4 tetrahedron exhibiting various types of disorder. The disorder of that tetrahedron is in $YbCd_6$ modeled by a cube with one-half occupancy of all vertices. In the case of YCd_6 the model is an icosahedron with one-third occupancy of all vertices. The discovery of the stable binary $MCd_{5.7}$ quasicrystals (M=Yb and Ca) (Refs. 7 and 8) has attracted the attention of the scientific community and generated a renewed interest in the RE-Cd systems. At the time of the finding of the $MCd_{5.7}$ quasicrystals, the structurally related MCd_6 phases were the highest known approximants. All reported binary alloys that have been described in literature to date with one (or several) of the three above-mentioned types of structures are summarized in Table I. The question that has puzzled many scientists since the finding of the $MCd_{5.7}$ phases is how an internally symmetry-breaking species such as the tetrahedron can be involved in the formation of these icosahedral quasicrystals.[23] The related paper by Takakura *et al.*[23] also handles the structures of the approximant phases $YbCd_6$ and $CaCd_6$, providing the Elser decomposition with the corresponding atomic decoration of the prolate rhombohedron which is one of the necessary constituents of the three-dimensional Penrose tiling that describes a quasicrystalline structure. Detailed studies of the tetrahedral disorder in the MCd_6 and newly found $M_{13}Cd_{76}$ approximants (M=Ca and Yb) can provide vital clues concerning the mechanisms implicated in the nucleation process of the $MCd_{5.7}$ phases.[24,25]

II. EXPERIMENT

Cd metal (splinters from a rod of pure metal, purified by melting) was mixed with chips of Pr, Nd, Sm, Eu, Gd, Dy, Yb, Y, and Ca (STREM, 99.9%) in the molar proportions $\sim$6:1 and sealed in stainless-steel ampoules. The ampoules were directly inserted into muffle furnaces at high tempera-

TABLE I. Previously reported structurally related binary alloys. Data sources: CRYSTMET (the metals database), *Binary Alloy Phase Diagrams*, and *Pearson's Handbook of Crystallographic Data for Intermetallic Phases* (Refs. 20–22).

Phase	Prototype structure	Reference
$CeCd_6$	YCd_6	9
$PrCd_6$	YCd_6	9
$NdCd_6$	YCd_6	10
$SmCd_6$	YCd_6	11
$EuCd_6$	YCd_6	12
$GdCd_6$	Ru_3Be_{17}, YCd_6	13
$TbCd_6$	YCd_6	1
$DyCd_6$	YCd_6	14
$HoCd_6$	YCd_6	9
$ErCd_6$	YCd_6	9
$TmCd_6$	YCd_6	9
$YbCd_6$	YCd_6, $YbCd_6$	5
$LuCd_6$	YCd_6	9
$NpCd_6$	YCd_6	15
$CaCd_6$	YCd_6	16
$SrCd_6$	YCd_6	16
YCd_6	YCd_6	4
Sc_3Zn_{17}	Ru_3Be_{17}	17
Ru_3Be_{17}	Ru_3Be_{17}	6
Yb_3Zn_{17}	Ru_3Be_{17}	18
Os_3Be_{17}	Ru_3Be_{17}	19

TABLE II. Experimental details.

Compound	Amount of M metal	Amount of Cd metal	Reaction temperature	Reaction time	Cooling rate
$Pr_3Cd_{18.18}$	Pr: 0.1695 g	Cd: 0.8335 g	605 °C	42 h	~3°/min
$NdCd_6$	Nd: 0.1442 g	Cd: 0.6743 g	595 °C	90 h	~3°/min
$SmCd_6$	Sm: 0.1810 g	Cd: 0.8264 g	720 °C	48 h	~1°/min
Eu_3Cd_9	Eu: 0.1926 g	Cd: 0.8065 g	665 °C	48 h	~3°/min
$GdCd_6$	Gd: 0.1573 g	Cd: 0.6744 g	700 °C	90 h	~3°/min
$DyCd_6$	Dy: 0.1906 g	Cd: 0.8115 g	720 °C	48 h	~1°/min
$YbCd_6$	Yb: 0.1731 g	Cd: 0.6747 g	595 °C	90 h	~3°/min
$CaCd_6$	Ca: 0.0412 g	Cd: 0.6549 g	550 °C	115 h	~3°/min
YCd_6	Y: 0.1535 g	Cd: 1.1644 g	690 °C	115 h	~3°/min

tures and heated to about 20 K below the reported melting points for each phase. After 40–115 h of isothermal heating, the furnaces were switched off and the samples were left inside to cool. Single crystals could easily be isolated from the resulting samples. The insides of the steel tubes were shiny, and showed no signs of any reaction with the mixture. All preparations were carried out in an inert atmosphere (argon) in order to avoid detrimental effects from water vapor or oxygen. All pertinent details of the experiments are given in Table II.

The single-crystal data was collected on a Stoe IPDS single-crystal x-ray diffractometer with a rotating anode Mo $K\alpha$ x-ray source operated at 45 kV and 90 mA. The single-crystal data collected for the refinement of the Pr-containing compound was collected on a Nonius Kappa charge-coupled device with a Mo $K\alpha$ x-ray source operated at 60 kV and 30 mA. The refinements of the structures were performed using the program JANA2000.[26] The unusually high R_{int} values for some of the collected single-crystal data (Table III below) are a result of the small size of the measured crystals (usually smaller than 60 μm; larger crystals were often twinned). The high redundancy of the measured reflections, however, also implies that the averaged intensities are reliable though the R_{int} values are high. The intensities of the reflections were integrated using Stoe software and the numerical absorption correction was performed with the programs X-RED and X-SHAPE.[27,28] The energy dispersive x-ray (EDX) analyses were carried out using a JEOL 820 scanning electron microscope at 20-kV accelerating voltage with the Si detector LINK AN10 000. Corrections were made for atomic number, absorption, and fluorescence. The electron-density isosurfaces were generated using the program JMAP3D.[29] The images were rendered using the programs TRUESPACE, version 5.2 and DIAMOND, version 2.1c.[30,31] EDX analysis was used solely to verify the absence of impurities (of mainly other RE elements) in the samples since the difference in composition between the $M\text{Cd}_{5.7}$ quasicrystals, and the $M\text{Cd}_6$ and $M_{13}\text{Cd}_{76}$ approximants is less than 1 at. %, which is below the margin of error for the instrument used. X-ray diffraction was used for phase identification. The compositions obtained from the EDX analyses did not contradict the results obtained in the final refinements. However, a small extra peak at 1.39 keV was observed in some of the crystals from the sample containing Pr; though the sample holder was made of Al it is impossible to exclude the presence of trace amounts of other RE elements in some of the crystals. The EDX analyses were in each case performed on approximately six different crystals from each synthesized sample. The crystals selected for diffraction experiments could themselves not be analyzed by EDX analysis since they were encapsulated in droplets of epoxy glue to protect them from the surrounding atmosphere. The compound Ce_6Cd_{37} was not synthesized as part of this investigation. The data used for the generation of isosurfaces for this compound was collected by Armbrüster and Lidin as part of a previously published work.[32]

III. STRUCTURAL DESCRIPTION

The coordination of Cd atoms around the different M metals in the $M\text{Cd}_6$ phases can be described with one single polyhedron, the $M\text{Cd}_{16}$ polyhedron (Fig. 1). It is a monocapped, double, pentagonal antiprism with nearly perfect fivefold symmetry. Twelve of these polyhedra are arranged to form the cluster unit that serves as the basic building block in

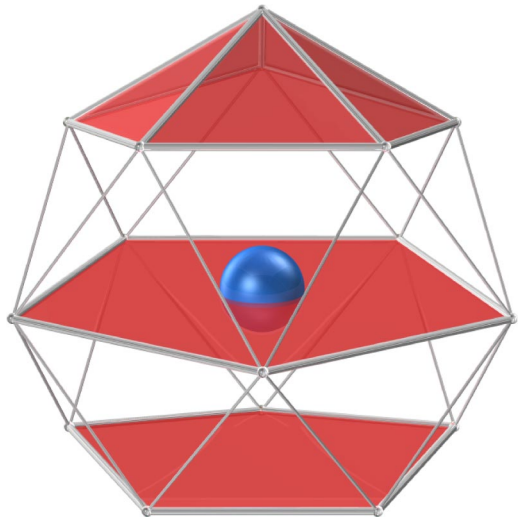

FIG. 1. (Color online) The $M\text{Cd}_{16}$ polyhedron. The M metal (large sphere) is surrounded by 16 Cd atoms forming a monocapped, double, pentagonal antiprism. The pentagonal planes and the pentagonal pyramid at the top of the polyhedron have been colored for clarity.

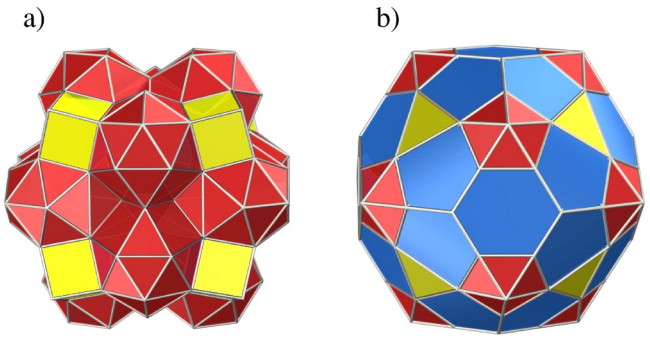

FIG. 2. (Color online) The basic building block of the $M\mathrm{Cd}_6$ phases. In (a) the cluster unit is built up of 12 $M\mathrm{Cd}_{16}$ polyhedra and eight Cd_8 cubes. In (b) we see the alternative representation of the basic building block. The defect triacontahedron is entirely composed of Cd atoms; the pentagonal pyramids seen in the image belong to the 12 underlying $M\mathrm{Cd}_{16}$ polyhedra (cf. Fig. 1). The bright triangular faces indicating missing corner atoms are in fact the planes that bisect the Cd_8 cubes seen in (a).

the $M\mathrm{Cd}_6$ and $M_{13}\mathrm{Cd}_{76}$ phases. This arrangement of $M\mathrm{Cd}_{16}$ polyhedra automatically generate cube-shaped interstices (Cd_8 cubes) that share square faces with the adjacent $M\mathrm{Cd}_{16}$ polyhedra. Each cluster unit is associated with eight surrounding Cd_8 cubes [Fig. 2(a)]. In order to visualize this in a more effective way and to enable us to describe the structures of the $M\mathrm{Cd}_6$ phases as a simple close packing of clusters, an alternative description of the cluster unit is preferable. The same cluster unit can be illustrated by connecting Cd atoms located at approximately the same distance from the center of the cluster to one another; the resulting polyhedron is a defect triacontahedron. This representation of the basic cluster unit is displayed in Fig. 2(b). Apart from the disordered and internally symmetry-breaking Cd_4 tetrahedron which forms the innermost and central component of the cluster unit, the subsequent Cd shells encountered going from the center to the periphery of the cluster are the pentagonal Cd_{20} dodecahedron [Fig. 3(a)], otherwise referred to as the dodecahedral cavity. This polyhedron is created by connecting the Cd atoms in the basal (un-capped) pentagonal planes of all 12 surrounding $M\mathrm{Cd}_{16}$ polyhedra to one another. The dodecahedron serves as a cage for the disordered Cd_4 tetrahedron. It is important to emphasize that this dodecahedron does not share any of its corners with the central Cd_4 tetrahedron; the two are completely disjoint. The next Cd shell is a Cd_{30} icosidodecahedron [Fig. 3(b)], composed of equilateral triangles and regular pentagons. This polyhedron is analogously created by connecting the intermediate pentagonal planes of the surrounding $M\mathrm{Cd}_{16}$ polyhedra to one another. The final and outermost Cd shell is the defect triacontahedron [Fig. 3(c) and Fig. 2(b)]. It is created by connecting the outermost pentagonal pyramids (capped pentagonal planes) of the surrounding $M\mathrm{Cd}_{16}$ polyhedra through the equidistant Cd atoms located in between them. The defects consist of missing corner atoms; this is illustrated as bright triangular faces on the triacontahedron. The construction of the basic cluster unit from concentric Cd shells is illustrated in Fig. 3. The structures of the $M\mathrm{Cd}_6$ phases can be described as a body-centered-cubic arrangement (bcc) of partially interpenetrating triacontahedral cluster units (Fig. 4). The Cd_8 cubes found in between the

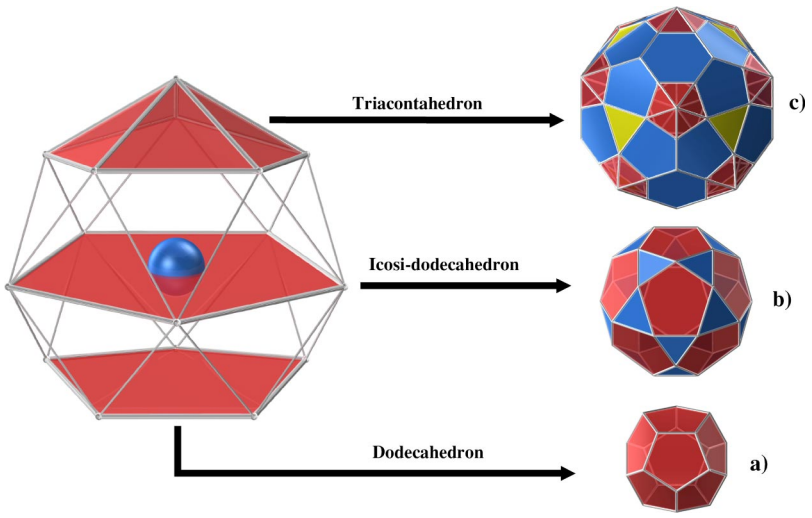

FIG. 3. (Color online) (Adapted from Ref. 24.) The Cd_{20} pentagonal dodecahedron is seen in (a); the Cd_4 tetrahedron residing inside has been omitted in the image. The Cd_{30} icosidodecahedron is seen in (b), and the 12 pentagons in the polyhedron correspond to the intermediate pentagonal planes of the surrounding $M\mathrm{Cd}_{16}$ polyhedra. Each of these pentagons has an M metal atom situated at their geometrical centers (seen as the large sphere in the magnified $M\mathrm{Cd}_{16}$ polyhedron to the left in the figure), but these atoms have been omitted in the image. The defect rhombic triacontahedron is seen in (c). The tips of the 12 $M\mathrm{Cd}_{16}$ polyhedra are seen as pentagonal pyramids.

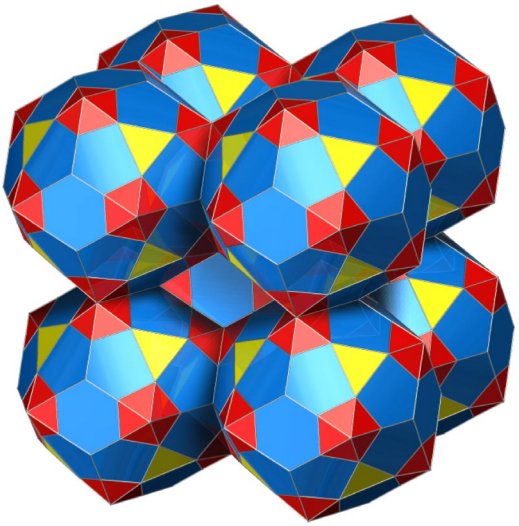

FIG. 4. (Color online) (Adapted from Ref. 24.) The structure of the $M\mathrm{Cd}_6$ phases can be displayed as a bcc packing of partially interpenetrating triacontahedral cluster units.

TABLE III. Refined atomic positions for the synthesized $M\mathrm{Cd}_6$ phases (M = Pr, Nd, Sm, Eu, Gd, Dy, Yb, Ca, and Y).

M	Atom	Wyck.	Occ.	x	y	z	U_{iso} (Å^2)
Pr	Cd1a	24*g*	0.101(3)	0	0.0854(8)	0.0768(8)	0.032(3)
Nd	Cd1a	24*g*	0.134(11)	0	0.0822(6)	0.0808(8)	0.040(5)
Sm	Cd1a	24*g*	0.170(16)	0	0.0811(10)	0.0816(11)	0.054(6)
Gd	Cd1a	24*g*	0.356(8)	0	0.0815(3)	0.0800(3)	0.091(2)
Dy	Cd1a	24*g*	0.223(6)	0	0.0819(9)	0.0816(10)	0.051(3)
Y	Cd1a	24*g*	0.092(11)	0	0.0749(13)	0.0889(13)	0.031(5)
Pr	Cd1b	48*h*	0.116(2)	0.0435(6)	0.0895(4)	0.0589(6)	0.050(2)
Nd	Cd1b	48*h*	0.099(6)	0.0376(10)	0.0899(5)	0.0627(7)	0.045(3)
Sm	Cd1b	48*h*	0.086(4)	0.0358(16)	0.0890(13)	0.0619(15)	0.050(4)
Eu	Cd1b	48*h*	1/6	0.0345(16)	0.083(2)	0.066(2)	0.086(10)
Dy	Cd1b	48*h*	0.072(4)	0.0357(19)	0.0928(14)	0.0549(19)	0.040(5)
Yb	Cd1b	48*h*	1/6	0.0282(7)	0.0801(11)	0.0754(12)	0.070(5)
Ca	Cd1b	48*h*	1/6	0.268(7)	0.0806(10)	0.0746(12)	0.062(5)
Y	Cd1b	48*h*	0.121(5)	0.0255(7)	0.0880(7)	0.0684(8)	0.048(3)
Pr	Cd2	24*g*	1	0	0.09162(6)	0.24221(7)	0.0306(3)
Nd	Cd2	24*g*	1	0	0.09211(5)	0.24114(7)	0.0251(3)
Sm	Cd2	24*g*	1	0	0.09217(10)	0.24083(14)	0.0368(5)
Eu	Cd2	24*g*	1	0	0.0912(3)	0.2426(3)	0.041(2)
Gd	Cd2	24*g*	1	0	0.09136(5)	0.23902(7)	0.0352(3)
Dy	Cd2	24*g*	1	0	0.09207(12)	0.24043(16)	0.0354(7)
Yb	Cd2	24*g*	1	0	0.09260(11)	0.23971(14)	0.0326(6)
Ca	Cd2	24*g*	1	0	0.09255(13)	0.23931(16)	0.0367(7)
Y	Cd2	24*g*	1	0	0.09224(8)	0.24067(11)	0.0300(4)
Pr	Cd3	16*f*	0.182(5)	0.1401(17)	0.1401(7)	0.1401(7)	0.043(3)
Eu	Cd3	16*f*	1/2	0.1285(14)	0.1285(14)	0.1285(14)	0.140(11)
Pr	Cd4	16*f*	0.818(5)	0.16218(14)	0.16218(14)	0.16218(14)	0.0361(5)
Nd	Cd4	16*f*	1	0.16095(4)	0.16095(4)	0.16095(4)	0.0239(2)
Sm	Cd4	16*f*	1	0.16108(8)	0.16108(8)	0.16108(8)	0.0305(3)
Eu	Cd4	16*f*	1/2	0.1584(9)	0.1584(9)	0.1584(9)	0.055(3)
Gd	Cd4	16*f*	1	0.16056(4)	0.16056(4)	0.16056(4)	0.0227(2)
Dy	Cd4	16*f*	1	0.16075(9)	0.16075(9)	0.16075(9)	0.0264(3)
Yb	Cd4	16*f*	1	0.16280(9)	0.16280(9)	0.16280(9)	0.0279(3)
Ca	Cd4	16*f*	1	0.16314(10)	0.16314(10)	0.16314(10)	0.0277(3)
Y	Cd4	16*f*	1	0.16083(6)	0.16083(6)	0.16083(6)	0.0211(2)
Pr	Cd5	8*c*	0.182(7)	1/4	1/4	1/4	0.0047(3)
Eu	Cd5	16*f*	1/2	0.235(3)	0.235(3)	0.235(3)	0.127(2)
Pr	Cd6	48*h*	1	0.19915(4)	0.34217(4)	0.11591(4)	0.0262(2)
Nd	Cd6	48*h*	1	0.20025(3)	0.34088(3)	0.11746(4)	0.0144(2)
Sm	Cd6	48*h*	1	0.20044(6)	0.34072(6)	0.11776(7)	0.0242(3)
Eu	Cd6	48*h*	1	0.1971(2)	0.3474(2)	0.1081(2)	0.035(1)
Gd	Cd6	48*h*	1	0.20018(3)	0.34058(3)	0.11665(3)	0.0192(2)
Dy	Cd6	48*h*	1	0.20044(8)	0.34059(8)	0.11815(8)	0.0215(3)
Yb	Cd6	48*h*	1	0.20002(7)	0.34235(7)	0.11633(7)	0.0206(3)
Ca	Cd6	48*h*	1	0.19985(8)	0.34191(8)	0.11671(8)	0.0217(4)
Y	Cd6	48*h*	1	0.20034(5)	0.34049(5)	0.11833(6)	0.0167(2)
Pr	Cd7	12*d*	1	0.40653(8)	0	0	0.0308(5)
Nd	Cd7	12*d*	1	0.40663(7)	0	0	0.0258(4)
Sm	Cd7	12*d*	1	0.40639(15)	0	0	0.0363(7)
Eu	Cd7	12*d*	1	0.4075(4)	0	0	0.042(2)
Gd	Cd7	12*d*	1	0.40611(7)	0	0	0.0281(3)
Dy	Cd7	12*d*	1	0.40554(17)	0	0	0.0323(9)
Yb	Cd7	12*d*	1	0.40753(15)	0	0	0.0276(8)

TABLE III. (*Continued*).

M	Atom	Wyck.	Occ.	*x*	*y*	*z*	U_{iso} (Å^2)
Ca	Cd7	12*d*	1	0.40758(17)	0	0	0.0301(9)
Y	Cd7	12*d*	1	0.40558(11)	0	0	0.0286(6)
Pr	Cd8	24*g*	1	0	0.34865(5)	0.40489(5)	0.0184(3)
Nd	Cd8	24*g*	1	0	0.34721(4)	0.40419(4)	0.0097(2)
Sm	Cd8	24*g*	1	0	0.34645(9)	0.40387(9)	0.0209(4)
Eu	Cd8	24*g*	1	0	0.3486(2)	0.4051(2)	0.029(1)
Gd	Cd8	24*g*	1	0	0.34535(4)	0.40387(4)	0.0166(2)
Dy	Cd8	24*g*	1	0	0.34571(11)	0.40432(10)	0.0174(5)
Yb	Cd8	24*g*	1	0	0.34366(10)	0.40421(9)	0.0145(4)
Ca	Cd8	24*g*	1	0	0.34316(11)	0.4042(1)	0.0158(5)
Y	Cd8	24*g*	1	0	0.34597(7)	0.40444(7)	0.0130(3)
Pr	Cd9	12*e*	1	0.19304(8)	1/2	0	0.0257(4)
Nd	Cd9	12*e*	1	0.19166(6)	1/2	0	0.0140(3)
Sm	Cd9	12*e*	1	0.19096(13)	1/2	0	0.0235(6)
Eu	Cd9	12*e*	1	0.1932(4)	1/2	0	0.032(2)
Gd	Cd9	12*e*	1	0.18975(6)	1/2	0	0.0197(3)
Dy	Cd9	12*e*	1	0.19041(16)	1/2	0	0.0204(7)
Yb	Cd9	12*e*	1	0.18721(13)	1/2	0	0.0181(6)
Ca	Cd9	12*e*	1	0.18616(15)	1/2	0	0.0191(8)
Y	Cd9	12*e*	1	0.19020(11)	1/2	0	0.0155(5)
Pr	Pr1	24*g*	1	0	0.29851(4)	0.19032(4)	0.0151(2)
Nd	Nd1	24*g*	1	0	0.29926(3)	0.18936(3)	0.0068(2)
Sm	Sm1	24*g*	1	0	0.29947(6)	0.18913(6)	0.0177(3)
Eu	Eu1	24*g*	1	0	0.2984(2)	0.18900(18)	0.0276(9)
Gd	Gd1	24*g*	1	0	0.29904(3)	0.18751(3)	0.0142(2)
Dy	Dy1	24*g*	1	0	0.29959(7)	0.18944(7)	0.0157(3)
Yb	Yb1	24*g*	1	0	0.30017(6)	0.18758(5)	0.0128(3)
Ca	Ca1	24*g*	1	0	0.3003(3)	0.1881(3)	0.0159(13)
Y	Y1	24*g*	1	0	0.29965(9)	0.18985(9)	0.0098(4)

MCd_{16} polyhedra [cf. Fig. 2(a)] were in the compounds in which M=Ce, Pr, and Eu observed to contain an additional Cd atom near their central position at the fractional coordinates $\frac{1}{4}\ \frac{1}{4}\ \frac{1}{4}$. The refined atomic positions for the investigated MCd_6 phases are summarized in Table III. Crystallographic data from the single-crystal refinements and final compositions are found in Table IV.

IV. RESULTS AND DISCUSSION

The single-crystal refinements made as part of this investigation show that deviations from the ideal and previously reported 1:6 stoichiometry of the so-called "MCd_6" phases are recurring. A report has already been made reassessing the structure of the compound formerly known as "$CeCd_6$," which more accurately should be referred to as Ce_6Cd_{37}.[32] The compositional differences between theinvestigated MCd_6 phases are caused by the additional Cd atoms located in some of the cube-shaped interstices present in all MCd_6, $RE_{13}(Cd/Zn)_{58}$, and $M_{13}Cd_{76}$ phases.[33,24] Partial occupation and even long-range ordering between these sometimes vacant, sometimes occupied cube-shaped interstices is known to occur; e.g., in the $RE_{13}(Cd/Zn)_{58}$-related compound $Dy_{13}Zn_{57}$ this metal vacancy ordering gives rise to a superstructure and a deviation from the ideal 13:58 composition.[33] Another example is the already-mentioned compound Ce_6Cd_{37} where exactly 50% of all cubic interstices are vacant. The vacancies in this compound are ordered so that every Cd_8 cube having a corner of the central Cd_4 tetrahedron pointing towards it will contract and consequently be vacant. This long-range order between vacant/occupied Cd_8 cubes and oriented Cd_4 tetrahedra is the direct cause for making the structure of Ce_6Cd_{37} primitive rather than body centered such as all other reported MCd_6 phases. The same kind of ordering could exist locally in the other compounds having additional Cd atoms in the Cd_8 cubes, however, no diffuse scattering was ever observed in the diffraction patterns collected from single-crystal x-ray data. Examples where significant electron densities have been observed and modeled with partially occupied atomic positions inside the Cd_8 cubes are the Pr- and Eu-containing phases described in this work and the structural analog to the compound $Ca_{13}Cd_{76}$ found in the Yb-Cd system.[25] The Cd_8 cubes share corners with the Cd_{20} dodecahedron; this shared corner atom is denoted Cd4 in Table III. As a result of the inherent disorder of the Cd_4 tetrahedron and the occasional occupation

TABLE IV. Crystallographic data for the refined structures.

Formula	$Pr_3Cd_{11\text{-}18}$	$NdCd_6$	$SmCd_6$	Eu_3Cd_{19}	$GdCd_6$	$DyCd_6$	$YbCd_6$	$CaCd_6$	YCd_6
Molar mass (g/mol)	2466.6	818.7	824.8	2591.5	831.7	836.9	847.4	714.54	763.3
Temperature of measurement (K)	293	293	293	293	293	293	293	293	293
Space group	*I m*-3	*I m*-3	*I m*-3	*I m*-3	*I m*-3	*I m*-3	*I m*-3	*I m*-3	*I m*-3
a axis (Å)	15.643(3)	15.605(2)	15.589(3)	15.958(3)	15.441(2)	15.462(2)	15.661(3)	15.702(3)	15.482(3)
Cell volume ($Å^3$)	3827.9(7)	3800.4(7)	3788.4(7)	4063.8(8)	3681.6(7)	3696.6(4)	3841.1(7)	3871.1(6)	3710.9(7)
z	8	24	24	8	24	24	24	24	24
F(000)	8398	8352	8400	8808	8474	8496	8592	7392	7848
Calculated density (g/cm^3)	8.557	8.583	8.677	8.472	9.000	9.023	8.793	7.354	8.197
Absorption coefficient	27.144	27.648	28.812	28.470	30.887	32.125	33.853	20.069	29.349
Rang of 2^{θ} (°)	4.51–27.38	3.3–52.1	4.4–51.8	2.55–28.33	3.3–52.1	3.7–52.2	3.7–51.8	4.4–51.8	1.84–25.52
Independent reflections	813	695	697	934	670	693	694	801	680
Observed reflections $[I>3^{\sigma}(I)]$	621	623	548	221	603	439	681	466	577
R_{int} (obs/all)	8.18/8.90	3.83/3.94	21.43/ 22.12	8.19/8.90	7.28/7.37	19.91/ 22.68	10.48/10.49	17.27/20.46	11.41/11.61
Number of parameters	52	47	48	48	46	47	48	48	46
*R*1	0.0262	0.0211	0.0401	0.0519	0.0199	0.0373	0.0396	0.0432	0.0316
*wR*2	0.0531	0.0524	0.0858	0.1090	0.0488	0.0720	0.0646	0.0847	0.0726
Absorption correction	Numerical, from shape	Numerical, from shape	Numerical, from shape	Numerical, from shape	Numerical, from shape	Numerical, from shape	Numerical, from shape	Numerical, from shape	Numerical, from shape
T_{min}, T_{max}	0.0237, 0.1027	0.4346, 0.7546	0.0425, 0.0952	0.0225, 0.0827	0.0291, 0.1158	0.0361, 0.1072	0.0142, 0.1001	0.0534, 0.1263	0.0527, 0.1441
$_{\Delta}\rho_{max}$, $_{\Delta}\rho_{min}$ (e/A^3)	3.23, −2.78	3.75, −2.45	3.21, −3.25	14.68, −14.48	1.89, −2.47	3.38, −3.78	4.65, −7.19	3.41, −3.77	3.22, −5.58
Δ/e.s.d	0.0003	0.0004	0.0003	0.0001	0.0004	0.0002	0.0002	0.0002	0.0003

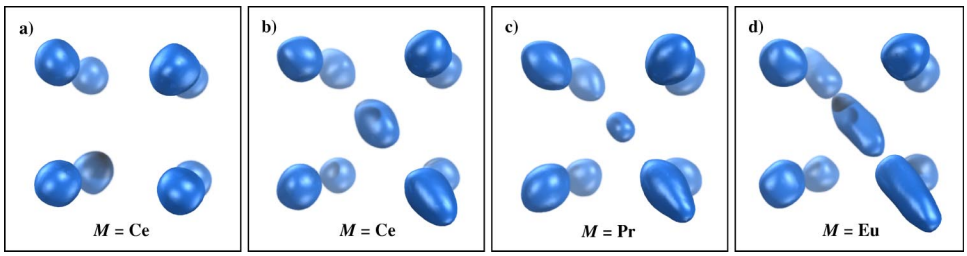

FIG. 5. (Color online) Electron density isosurfaces at the 10-$e/Å^3$ level in the location of the Cd_8 cubes. The surfaces displayed in (a) through (d) have been generated from F_{obs} data originating from the individual single-crystal measurements. (a) and (b) The symmetry-independent vacant and fully occupied cubes, respectively, of the compound Ce_6Cd_{37}. (c) The appearance of the symmetry-equivalent cubes in the compound $Pr_3Cd_{18.18}$. The additional Cd position is only ~18% occupied but is clearly visible. The image also shows the slight elongation of the atoms along the space diagonal to the cube, resulting in pear-shaped corner atoms. (d) The appearance of the cubes in the compound Eu_3Cd_{19}. The cubes contain three extremely elongated atoms modeled by split positions with half occupancy. This diagonal disorder is accentuated with increasing Cd content inside the Cd_8 cubes.

of the Cd_8 cubes by an additional Cd atom, the Cd_{20} dodecahedron and thus the Cd_8 cubes are distorted. This induces a disorder on the Cd4 position that can be viewed as elongations in the Fourier maps (see Fig. 5). These elongations become more prominent the higher the occupation of the interstitial position. The best way to model this disorder in the refinements was by introducing an extra split position adjacent to Cd4. This position is denoted Cd3 in Table III, and it is only occupied in the cases in which we have an atom inside the Cd_8 cube. This disorder propagates diagonally (in the [111] direction) throughout the cubic unit cell by also affecting the relative orientation and thus the disorder of the adjacent Cd_4 tetrahedra in order to avoid too short Cd-Cd distances. Three-dimensional Fourier maps showing the electron densities calculated from experimental data in the location of the Cd_8 cubes for the phases with $M=$ Ce, Pr, and Eu are displayed in Figs. 5(a) through 5(d).

The additional Cd atoms occasionally located inside the Cd_8 cubes and the absence of the entire Cd_4 tetrahedron in the phases that have been assigned to the structure Ru_3Be_{17}, (cf. Table I) are the two items solely responsible for the deviations from the ideal 1:6 stoichiometry of all the reported MCd_6 phases. In Table III these atomic positions are denoted Cd1a and Cd1b for atoms comprising the Cd_4 tetrahedron, and Cd5 for the additional position inside the Cd_8 cubes. In most cases the refinements made as part of this work showed no significant electron densities inside the Cd_8 cubes, thus the 1:6 stoichiometry is maintained. In addition to the already known case of Ce_6Cd_{37}, Fig. 5 clearly shows that significant electron densities are also found inside the Cd_8 cubes of the Pr- and Eu-containing phases, resulting in the final compositions $Pr_3Cd_{18.18}$ and Eu_3Cd_{19}. Several measurements were made on different single crystals of the Pr-containing phase and the refinements all indicated nonzero occupancy of the Cd5 position. However, the occupancy of this atomic position was found to vary greatly. The final refined compositions all arrived within the hypothetical predominance area given by $Pr_3Cd_{18+\delta}$ $(0\leqslant\delta\leqslant 1)$, where $\delta=1$ corresponds to completely filled Cd_8 cubes. The variations in Cd content were accompanied by subsequent variations in the cubic cell parameter that reached a maximum value of 15.955(2) Å for a single crystal with the refined composition Pr_3Cd_{19} $(\delta=1)$. However, the actual range of the suggested solid solution is yet to be explored. For convenience, however, the term "MCd_6" is still used in this work when referring to these related compounds with a common name, though not in the strict compositional sense.

Upon longer exposure to x rays the Eu-containing phase showed weak superstructure reflections corresponding to an F-centered cubic lattice with a doubled cell parameter. These results have, due to their complexity, been excluded from this study and are presented in a separate work.[34] All data concerning the Eu-containing compound herein presented as Eu_3Cd_{19} are solely related to the substructure of this compound and should thus be interpreted as such. The fact that the standard deviations for the different atomic positions and the residual electron densities from the refinement of Eu_3Cd_{19} are generally much greater than for the other presented compounds (Table III) clearly indicates that the substructure alone fails to describe this compound in a satisfactory way. These results have still been included in this work to show the clear structural kinship between the Eu-containing phase and the other MCd_6 compounds. Nothing indicating the presence of a superstructure was seen in the diffraction data collected for the Pr-containing compounds.

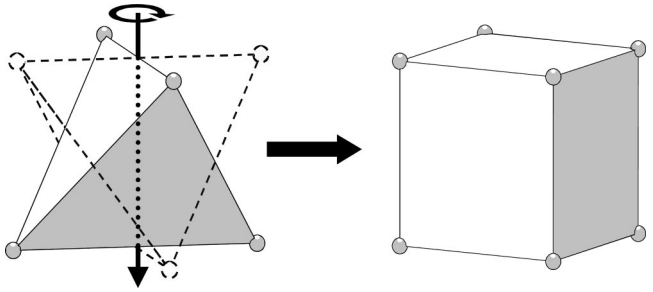

FIG. 6. (Color online) Schematic representation of type-1 disorder; a 90° rotational disorder along the inherent twofold axis of the tetrahedron, resulting in a cube with half-occupied corner positions.

Two types of disorder, which may or may not coexist, can mainly be used to describe the Cd_4 tetrahedra of the MCd_6 phases. Type 1 is a 90° rotational disorder of the whole tetrahedron along its inherent twofold axis resulting in an image of a semioccupied cube in the electron-density maps (Fig. 6). Type 2 is a triple split of the tetrahedral corner positions as a result of the corner atoms' off-center displacement from the space diagonal to the cubic unit cell (Fig. 7). The atomic position affected by the triple split is denoted Cd1b in Table III. On a sufficiently large split, an intermediate state will be reached where the obtained coordination polyhedron will have the appearance of a cube octahedron. At this stage it is impossible to determine whether only the type-2 disorder is present, or both type 2 and type 1. This is a consequence of the inherent fourfold rotational axis of the cube octahedron, in other words the same cube octahedron can be obtained by increasing the triple split or triangular faces of a truncated cube. The atomic position that generates the corners of the cube octahedron is denoted Cd1a in Table III. If the triple split is further increased; it will give the effect of pseudo rotation. The whole procedure is schemati-

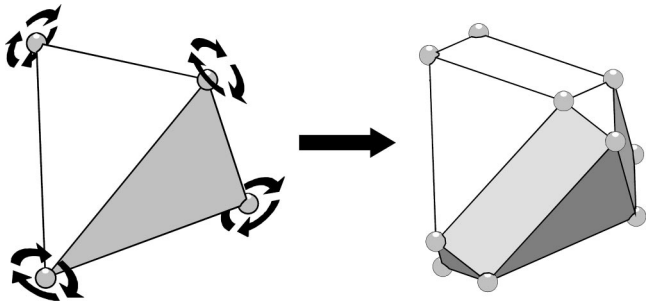

FIG. 7. (Color online) Type-2 disorder, arising when the inherent threefold axis of the tetrahedron fails to coincide with the space diagonal to the cubic unit cell. The result is a triple split of the tetrahedral corner atoms. The amount of splitting can be defined as the distance between these three corner atoms.

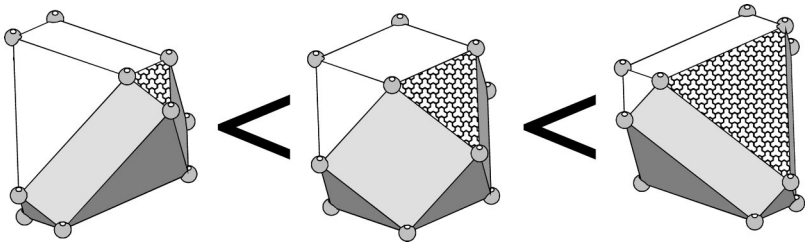

FIG. 8. (Color online) The effect of pseudorotation is obtained by successively increasing the amount of the split in the type-2 disorder. This is seen as an increase in the area of the patterned triangular face on the three polyhedra in the figure. The polyhedron to the far right is identical to the one on the far left but rotated 90°. The intermediate cube octahedron is seen in the middle.

cally represented in Fig. 8. The model of the disordered tetrahedron is justified by the fact that any other polyhedron constructed from the observed electron densities would yield unreasonably short Cd-Cd distances. Furthermore, the sum of refined occupancies in all cases adds up to four Cd atoms inside the dodecahedral cavity in the different refinements. Three-dimensional electron-density isosurfaces have been generated from the collected single-crystal data for the different $M\mathrm{Cd}_6$ phases. The results showing the measured electron densities corresponding to the disordered tetrahedra located inside the different dodecahedral cavities of the investigated compounds are displayed in Fig. 9.

The $M_{13}\mathrm{Cd}_{76}$ phases are structurally closely related to the $M\mathrm{Cd}_6$ phases; the same basic structural building blocks can be used to describe these compounds and both structure types are essentially close packings of similar cluster units composed of spherical Cd shells with icosahedral symmetry.[24] An object with icosahedral symmetry must by definition possess fivefold, threefold, and twofold axes of rotation. The $M\mathrm{Cd}_{5.7}$ quasicrystals have been identified as icosahedral by electron-diffraction studies,[7,8] but how the central tetrahedron fits into this structural view is still unclear.[23] In conclusion the studies on the $M\mathrm{Cd}_6$ phases presented in this work show that the disorder of these compounds is not random and the icosahedral symmetry is still broken in spite of the tetrahedral disorder. It is also obvious that though the structural kinship between the different $M\mathrm{Cd}_6$ phases is obvious, they are not isostructural and the three prototype structures assigned to these phases fail to accurately describe them in a satisfactory way since various forms of tetrahedral disorder exist and in some cases additional Cd atoms are found in the cubic interstices. Moreover, the structural description of the species residing within the dodecahedral cavity of the two prototype structures YbCd_6 and YCd_6 finds little support in the single-crystal data collected for these compounds as part of this work. In YbCd_6 the disordered Cd_4 tetrahedron was modeled by a cube with one-half occupancy of all vertices in the original paper, not taking into account the variable triple split seen in Fig. 9(h). In YCd_6 the disordered Cd_4 tetrahedron was modeled by an icosahedron with one-third occupancy of all vertices in the original paper. It is a well-known fact that an icosahedron can easily be transformed into a cube octahedron by a minor

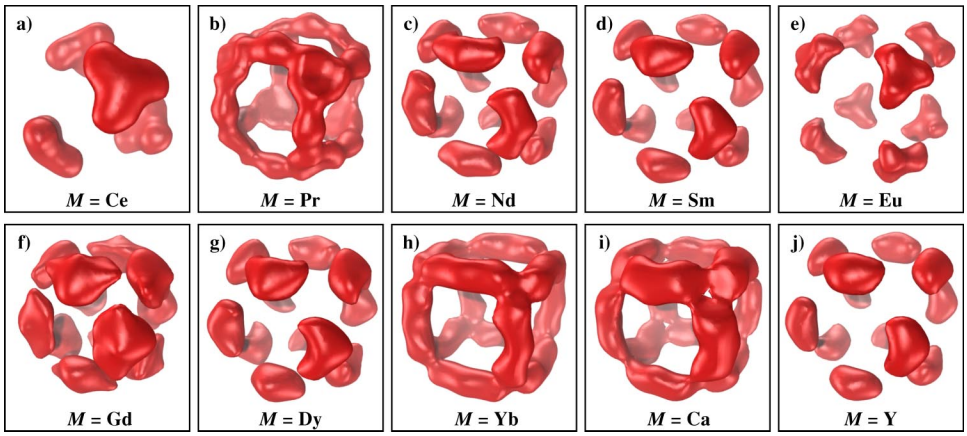

FIG. 9. (Color online) Electron-density isosurfaces at the 8.5-$e/\text{Å}^3$ level in the location of the Cd_4 tetrahedra, inside the dodecahedral cavities of the different $M\mathrm{Cd}_6$ phases. The surfaces displayed in the figure have been generated from F_{obs} data originating from the individual single-crystal measurements. The maps clearly show the differences in the disorder of the Cd_4 tetrahedron between the investigated $M\mathrm{Cd}_6$ phases. (a) The tetrahedron of $\mathrm{Ce}_6\mathrm{Cd}_{37}$, displaying only type-2 disorder (see Fig. 7). When type-1 (see Fig. 6) and type-2 disorders are combined the resulting polyhedron is a truncated cube; this is the case for the compound $\mathrm{Eu}_3\mathrm{Cd}_{19}$ seen in (e). The same phenomenon is seen in (b), (h) and (i) where the Cd_4 tetrahedra for the compounds $\mathrm{Pr}_3\mathrm{Cd}_{18.18}$, YbCd_6, and CaCd_6, respectively are displayed, with the important addition of variability in the triple split manifesting itself as smeared out electron densities. In (b) it is particularly apparent that besides the type-1 and type-2 disorders an additional atom is seen at the position forming a cube octahedron (Cd1a). This position is also occupied in the $M\mathrm{Cd}_6$ phases where $M=$ Nd, Sm, Gd, Dy, and Y. The variation in the triple split causes the crescent-shaped electron densities seen in (c), (d), (f), (g), and (j). All atoms in the Cd1a and Cd1b positions were refined isotropically except for the compound GdCd_6 where the irregular shape of the atoms in the resulting cube octahedron was modeled with anisotropic temperature parameters. Only the equivalent isotropic temperature parameters are displayed in Table III.

distortion. This description would be more appropriate but large anisotropic temperature parameters or higher-order anharmonic tensors would be required in order to model the crescent-shaped electron-density distributions seen in Fig. 9(j). The model presented in this work uses a split position approach to model these electron densities. The collected single-crystal data indicate a nonstoichiometry for the Pr-containing phase, giving a predominance area between the two end members $PrCd_6$ and Pr_3Cd_{19}. Weak superstructure reflections were observed in the data collected for the Eu-containing compound, as well as significant electron densities inside the Cd_8 cubes.

ACKNOWLEDGMENTS

This study has been financially supported by the Swedish Natural Science Research Council and the Foundation for Strategic Research.

*Author to whom correspondence should be addressed. FAX: +46-8-15 21 87. Email address: cesar@inorg.su.se

[1] G. Bruzzone, M. L. Fornasini, and F. Merlo, J. Less-Common Met. **30**, 361 (1973).
[2] F. E. Wang, Acta Crystallogr. **22**, 579 (1967).
[3] D. Shechtman, I. Blech, D. Gratias, and J. W. Cahn, Phys. Rev. Lett. **53**, 1951 (1984).
[4] A. C. Larson and D. T. Cromer, Acta Crystallogr., Sect. B: Struct. Crystallogr. Cryst. Chem. **27B**, 1875 (1971).
[5] A. Palenzona, J. Less-Common Met. **25**, 367 (1971).
[6] D. E. Sands, Q. C. Johnson, O. H. Krikorian, and K. L. Kromholtz, Acta Crystallogr. **15**, 1191 (1962).
[7] A. P. Tsai, J. Q. Guo, E. Abe, H. Takakura, and T. J. Sato, Nature (London) **408**, 537 (2000).
[8] J. Q. Guo, E. Abe, and A. P. Tsai, Phys. Rev. B **62**, R14 605 (2000).
[9] I. Johnson, R. Schablaske, B. Tani, and K. Anderson, Trans. Metall. Soc. AIME **230**, 1485 (1964).
[10] I. Johnson, K. E. Anderson, and R. A. Blomquist, ASM Trans. Q. **59**, 3520 (1966).
[11] G. Bruzzone and M. L. Fornasini, J. Less-Common Met. **37**, 289 (1974).
[12] K. H. J. Buschow and F. J. van Steenwijk, Physica B & C **85B**, 122 (1977).
[13] G. Bruzzone, M. L. Fornasini, and F. Merlo, J. Less-Common Met. **25**, 295 (1971).
[14] T. Dagerhamn, Chem. Commun. Univ. Stockholm **N05**, 1 (1978).
[15] M. Krumpelt, I. Johnson, and J. J. Heiberger, J. Less-Common Met. **18**, 35 (1969).
[16] G. Bruzzone, Gazz. Chim. Ital. **102**, 234 (1972).
[17] R. I. Andrusyak, B. Y. A. Kotur, and V. E. Zavodnik, Kristallografiya **34**, 996 (1989).
[18] G. Bruzzone, M. L. Fornasini, and F. Merlo, J. Less-Common Met. **22**, 253 (1970).
[19] N. N. Matyushenko, L. F. Verkhorobin, V. P. Serykh, and N. S. Pugachev, Russ. Metall. **6**, 146 (1982).
[20] Computer code CRYSTMET, version 1.0 (Toth Information Systems Inc., Ottawa, Canada, 1999).
[21] *Binary Alloy Phase Diagrams*, 2nd ed. (American Society for Metals, Metals Park, OH, 1996).
[22] P. Villars and L. D. Calvert, *Pearson's Handbook of Crystallographic Data For Intermetallic Phases*, 2nd ed. (American Society for Metals, Metals Park, OH, 1991).
[23] H. Takakura, J. Guo, and A. P. Tsai, Philos. Mag. Lett. **81**, 411 (2001).
[24] C. P. Gómez and S. Lidin, Angew. Chem., Int. Ed. Engl. **40**, 4037 (2001).
[25] C. P. Gómez (unpublished).
[26] V. Petříček and M. Dusek, computer code JANA2000 (Institute of Physics AVCR, Praha, Czech Republic, 2002).
[27] Computer code X-RED, version 1.07 (Stoe and Cie GmbH, Darmstadt, Germany, 1996).
[28] Computer code X-SHAPE, version 1.01 (Stoe and Cie GmbH, Darmstadt, Germany, 1996).
[29] S. Weber, computer code JMAP3D (NIRIM, Tsukuba, Japan, 1999).
[30] R. Ormandy, computer code TRUESPACE, version 5.2 (Caligari Corporation, Mountain View, USA, 2000).
[31] K. Brandenburg, computer code DIAMOND, version 2.1c (Crystal Impact, Bonn, Germany, 1999).
[32] M. Armbrüster and S. Lidin, J. Alloys Compd. **307**, 141 (2000).
[33] C. P. Gómez and S. Lidin, Solid State Sci. **4**, 901 (2002).
[34] C. P. Gómez and S. Lidin (unpublished).